Mobile measurement setup according to IEC 62220-1-2 for DQE determination on digital mammography systems

Matthias B. Greiter*[a], Christoph Hoeschen[a]

[a]Helmholtz Zentrum München, German Research Center for Environmental Health, Institute of Radiation Protection, Ingolstädter Landstr. 1, 85764 Neuherberg, Germany

ABSTRACT

The international standard IEC 62220-1-2 defines the measurement procedure for determination of the detective quantum efficiency (DQE) of digital x-ray imaging devices used in mammography. A mobile setup complying to this standard and adaptable to most current systems was constructed in the Helmholtz Zentrum München to allow for an objective technical comparison of current full field digital mammography units employed in mammography screening in Germany.

This article demonstrates the setup's capabilities with a focus on the measurement uncertainties of all quantities contributing to DQE measurements. Evaluation of uncertainties encompasses results from measurements on a Sectra Microdose Mammography in clinical use, as well as on a prototype of a Fujifilm Amulet system at various radiation qualities. Both systems have a high spatial resolution of 50 µm x 50 µm. The modulation transfer function (MTF), noise power spectrum (NPS) and DQE of the Sectra MDM are presented in comparison to results previously published by other authors.

Keywords: DQE, mammography, MTF, NPS

1. INTRODUCTION

Determination of detective quantum efficiency (DQE) is one possibility to assess image quality of digital x-ray devices. DQE describes how efficient a detector uses incoming quanta for generating an image. It comprises the dose used for image generation, the investigated system's noise power spectrum (NPS), and its modulation transfer function (MTF). One advantage less elaborate, phantom image, and human observer-based means of image quality assessment is the objective quality of DQE measurement, since the evaluation is dominated by specified mathematical operations rather than human perception.

This perception-independence of the DQE makes it an attractive quantity for comparison of different systems. However, measurements made by different groups under individual circumstances and with non-standardized phantoms tend to give different results. One example is the NPS and MTF determination on a Sectra Microdose Mammography system by Monnin et al.[1] and the evaluation by Honey et al.[2]. MTF results are slightly lower on average in the latter publication, but still show the same dependence on spatial frequency. In contrast, only Honey et al. find very high NPS values for low spatial frequencies, and a pronounced peak in one direction, while Monnin et al. instead observe a different slope of the NPS curves of both directions.

Such differences call for a standardized measurement procedure, as it is recommended in the International Electrotechnical Commission's (IEC) series of international standards concerned with DQE measurement, of which IEC 62220-1-2[3] is focused on mammography. This standard includes the requirement to state measurement uncertainties, which are often not in the focus of publications presenting DQE measurement. Still, they are important to judge whether observed discrepancies between results may be attributed to small random effects, or hint at a systematic difference between two systems thought of as identical in construction. The determination of uncertainties in DQE measurements according to IEC 62220-1-2 will be a main part of the results presented here.

*matthias.greiter@helmholtz-muenchen.de

Medical Imaging 2010: Physics of Medical Imaging, edited by Ehsan Samei, Norbert J. Pelc,
Proc. of SPIE Vol. 7622, 76224P · © 2010 SPIE · CCC code: 1605-7422/10/$18 · doi: 10.1117/12.844196

2. MEASUREMENT SETUP

The measurement setup consists of four essential sub-units. A light-weight stand provides fittings for a mounting frame and an ionization chamber (figure 1), both of which can adjusted laterally and radially, as well as tilted to a lesser degree. By use of the stand, the setup can be adapted to any mammography system with sufficient space between x-ray source and detector, since no coupling to the x-ray source unit is necessary. A steel edge phantom for MTF measurements placed in an aluminum frame completes the setup (figure 2).

The mounting frame features three parallel layers into which several items can be optionally set in an inner frame of 150 mm x 150 mm:

- An additional filter of 2.00 mm Al (purity 99.999%) as required for the radiation qualities in IEC 62220-1-2,
- sets of high purity Al plates and foils as half-value layers (HVL),
- a pair of identical double wire crosshairs to test the beam geometry both of light and x-rays.

The frame also supports two perpendicular pairs of stainless steel plates which are used as collimators. Each of the stainless steel plates has a transmission of $\leq 10^{-5}$ for mammographic x-ray spectra up to 35 kVp.

A flat ionization chamber (M 23344 – 147, 0.2 mm^3 volume; PTW-Freiburg, Germany) and an electrometer (UNIDOS 11024, PTW-Freiburg, Germany) are provided for dosimetry, i.e. air kerma measurement. The combination of these instruments was previously calibrated in the WHO/IAEA Secondary Standard Dosimetry Laboratory at the Helmholtz Zentrum München, Germany. Stainless steel plates covering the ionization chamber and its mounting are included to allow measuring backscattered radiation while suppressing direct radiation. The measurement should take place in the image plane with the detector removed. If this is not possible, air kerma must be measured between source and detector, and corrections for geometry, absorption between ionization chamber and detector, and backscattered radiation must be applied.

The MTF phantom frame is designed to reproducibly and precisely adjust the edge phantom on most common detectors. Its combination of hooks and screws makes it possible to remove and remount frame and phantom for repeated measurements without the need for readjustment. The frame is supported by three screws with plastic caps and can be tilted freely by small angles. The edge phantom is a stainless steel plate of 0.8 mm thickness as recommended in IEC 62220-1-2, with a polished edge perpendicular to the plate. It can be rotated freely in an inner frame to allow for any angle between pixel array and edge. The inner frame can be rotated by 90° to easily achieve an almost identical edge angle in all directions.

Using a water gauge and rulers with slots visible in x-ray images, it is possible to adjust the placement of most parts with uncertainties of 1 mm or less. The complete setup, including all measuring equipment, can be transported and operated by a single person.

Adaptation of the setup to the investigated systems is described below in section 4.

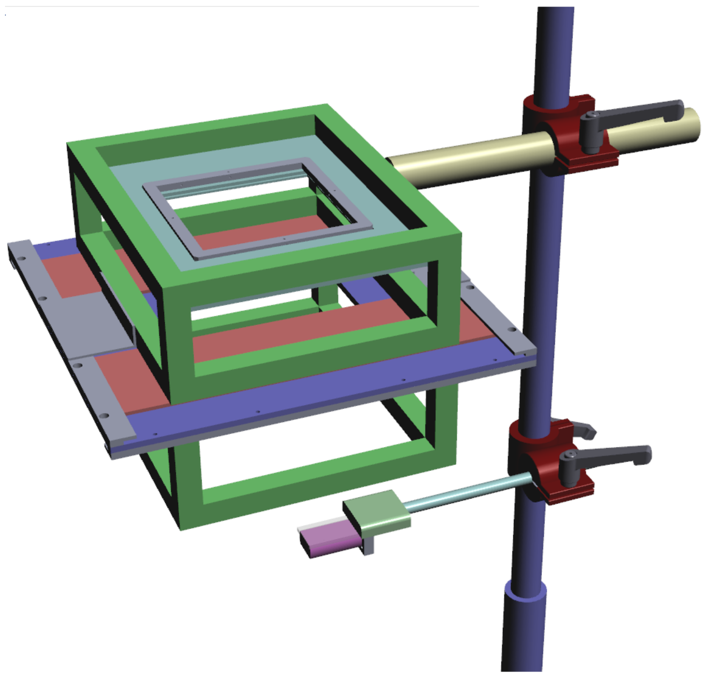

Figure 1: Schematic view of the mounting frame for beam-shaping, additional filters and crosshairs (upper part) and ionization chamber (lower part).

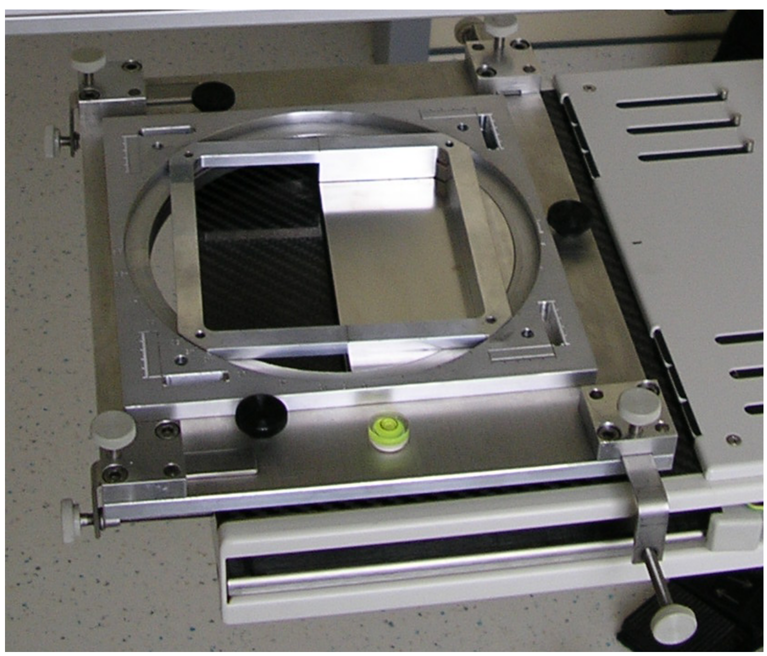

Figure 2: MTF edge phantom in its frame.

3. DATA EVALUATION

The model equation for calculating the DQE in IEC 62220-1-2 is:

$$DQE(u,v) = MTF^2(u,v)\frac{K_a \cdot SNR_{in}^2}{NPS_{out}(u,v)} \tag{1}$$

Squared signal-to-noise ratio per air kerma SNR_{in}^2 can be adopted from IEC standards, or must be calculated if it is unknown for the investigated radiation quality. Air kerma K_a is measured directly, while MTF and NPS are determined from image data. The respective uncertainties of these quantities all contribute to the combined uncertainty according to the recommendations of the "Guide to the expression of uncertainty in measurement" (GUM)[4], most easily expressed as relative uncertainties u_r:

$$u_{r,DQE} = \sqrt{4 \cdot u_{r,MTF}^2 + u_{r,Ka}^2 + u_{r,SNRin2}^2 + u_{r,NPS}^2} \tag{2}$$

"Expanded" uncertainty is defined by the GUM as a multiple of combined uncertainty with a coverage factor, thus encompassing a larger "fraction of the distribution of values that could reasonably be attributed to the measurand". IEC 62220-1-2 requires stating the expanded uncertainty of the DQE with a coverage factor of 2. In contrast, all uncertainties discussed in the following sections are listed with a coverage factor of 1 unless otherwise stated.

3.1 Air kerma K_a

Air kerma measurements with ionization chambers require several corrections and scaling factors, especially if the imaging detector cannot be removed for the measurement:

$$K_a = C \cdot N_k \cdot k_Q \cdot k_\rho \cdot k_{Pos} \cdot k_{Abs} \cdot k_S \tag{3}$$

C	Charge measured by the ionization chamber and electrometer
N_k	Calibration factor of the measurement equipment, taken from its calibration certificate
k_Q	Correction factor for radiation quality as previously calibrated
k_ρ	Correction factor for air density, including temperature and atmospheric pressure
k_{Pos}	Correction factor for ionization chamber position, specific for each measured geometry
k_{Abs}	Correction factor for x-ray absorption in the air layer between ionization chamber and image plane
k_S	Correction for backscattered radiation

The uncertainties of C, N_k, k_Q, and k_ρ were derived from the respective instruments' documentations and calibration certificates according to the values measured in the respective investigations. Using the x-ray facilities of the WHO/IAEA Secondary Standard Dosimetry Laboratory of the Helmholtz Zentrum München, a test source, and a second calibrated ionization chamber (Radcal 2026 C / 6 M), N_k and k_Q were furthermore controlled preceding the measurements.

All further correction factors had to be determined for each instrumental setup, since they depend on the individual position of the ionization chamber, ambient climatic conditions, as well as the composition and geometry of the detector in case of backscatter.

- k_{Pos} was calculated from the distances between focus and detector and between focus and ionization chamber, using the inverse square law for point sources.
- k_{Abs} is an estimate of the relative transmission of the air layer between chamber position and image plane. X-ray mass-energy absorption coefficients from NIST[5] for air and aluminum were interpolated to the necessary energy resolution using power functions in order to calculate layer transmissions. The effective x-ray energy needed for this estimation was derived from the measured aluminum half-value layer thickness.
- The backscatter correction factor k_S was estimated from measurements at high dose with and without direct radiation to the ionization chamber. Direct radiation of low-energy x-rays can be effectively shielded by a 3 mm plate of stainless steel covering the ionization chamber.

The respective uncertainties of k_{Pos}, k_{Abs}, and k_S were estimated from the uncertainties of the respective distance and dose measurements, and from slight variations of the parameters used in transmission calculations.

3.2 Squared signal-to-noise ratio per air kerma SNR_{in}^2

IEC 62220-1-2 includes tabulated values of SNR_{in}^2 for several radiation qualities, but it does not list uncertainties. If a measured radiation quality matches one of the listed qualities, SNR_{in}^2 may be adopted as a constant with negligible uncertainty. However, differences in voltage or half-value layer lead to deviations in the x-ray spectra and consequentially also in SNR_{in}^2, necessitating a possibility to calculate the latter for additional radiation qualities. We used a spectral simulation software based on data from IPEM Report 78[6, 7]. Calculations for the spectra in IEC 62220-1-2 resulted in slightly different values both for the expected half-value layers of aluminum and for SNR_{in}^2, which was expected from a comparison of spectral simulation codes published by Meyer et al.[8]. In order to retain comparability with the IEC standard, all HVL and SNR_{in}^2 results were scaled to the most similar IEC-listed radiation quality. In this way, the relative uncertainty of SNR_{in}^2 can be derived from small variations in the relevant input parameters (e.g. tolerances in inherent filtering given by a system's manufacturer, tolerance of added aluminum filtering, air layer thickness, anode angle, and variations in voltage). The relative uncertainties for different radiation qualities obtained in this way are 0.3 – 0.5 % (coverage factor of 1), in contrast to a deviation of 1 – 2 % between the IEC values and the raw results, and to the even larger deviations observed in the publication of Meyer et al.

3.3 MTF and NPS

All images used to calculate MTF and NPS were linearized prior to the calculation, i.e. raw pixel values were converted to photon fluence. MTF and NPS were calculated by procedures written in IDL (Interactive data language, ITT Visual Information Solutions, Boulder, CO, US) by E. Buhr and H. Illers, PTB, Braunschweig, Germany, and modified by the authors. These procedures adopt the IEC recommendations step-by-step and shall only be briefly described here.

Oversampled edge profiles are obtained from a 25 mm x 50 mm sized region of interest (ROI) in linearized edge images. An average of these profiles is then differentiated, subjected to a fourier transform, and normalized to its value at zero spatial frequency to obtain the pre-sampling MTF. Corrections are included as recommended for the finite-element differentiation, and for the frequency-axis scaling due to the small angle between edge and pixel matrix.

The two-dimensional NPS is calculated from a ROI of approximately 50 mm x 50 mm. Large-area variation is compensated by the subtraction of a two-dimensional second-order polynomial from the linearized data of the whole ROI. Sections of 256 x 256 pixels, overlapping by 128 pixels in each direction are fourier-transformed. Each complete evaluation includes ROIs from several images with at least 4 million pixels. The two-dimensional NPS results are then averaged. One-dimensional NPS values are obtained from this average spectrum by averaging 14 rows or columns around the frequency axes, excluding the axes themselves.

The resulting MTF and NPS curves have a fine resolution, i.e. 128 data points for NPS curves and up to ~500 for MTF curves per axis. According to IEC 62220-1-2, NPS and MTF results shall be binned around spatial frequencies of multiples of 0.5 mm^{-1}. Binning reduces noise, but also can mask peaks on systems like the Sectra MDM as referred to in the introduction.

If the curves are flat within a bin, the standard deviation of the mean (SDM) of the contributing values can be used as measure of uncertainty as recommended by the GUM. However, MTF and in several cases NPS are clearly frequency-dependent, and the use of the SDM would overestimate the uncertainty, i.e. the random deviation of individual data points from their unknown frequency-dependent expected value. Therefore, the uncertainties presented hereafter are based on squared deviations from locally linear approximated curves rather than from the constant value of the bin mean. Approximation is necessary since no actual functional relation is known to which the curves could be globally fitted. The slope of the linear approximation was determined from directly adjacent bins of the same width, which, depending on their width, need not be identical to the IEC bins. The offset was determined by the respective central bin mean, which should lie on the approximated line. This method is suitable for most smooth MTF and NPS curves, since they can be well approximated. In case of large curvature, affected bins must be treated individually. Bins near zero or Nyquist frequency may also have to be treated specially, if too few neighboring values are available. In such cases, the standard deviation of the mean was used, accepting the overestimation of uncertainty.

4. RESULTS AND DISCUSSION

4.1 Investigated systems

Two full-field digital mammography systems were evaluated with the setup described above.

For the first, a Fujifilm Amulet prototype, only measurement uncertainties are presented in this article. The measurements on this prototype were made twice during its adaptation process to the European market, with ongoing changes of the system software and calibration. No NPS, MTF or DQE results will be shown here, since they are subject to future change; however, their uncertainties were unaffected by the systems developmental changes.

The Amulet features typical flat-field geometry with ample space between x-ray source and detector platform. The system can generate x-rays from molybdenum or tungsten anodes and uses molybdenum or rhodium filters. The Amulet's detector is based on a double layer of amorphous selenium with a pixel size of 50 µm x 50 µm[9]. Instead of using TFTs, it controls the pixel readout by selective optical irradiation of the lower layer of a-Se, a technique Fujifilm calls 'Direct Optical Switching'. The detector of the investigated system had a size of 177 mm x 237 mm with 3540 x 4740 pixels. The recorded bit depth was 14 bit.

Results were obtained for three radiation qualities, Mo/Mo at 28 kV and W/Rh at 28 kV from an initial measurement, and W/Rh at 29 kV from a later measurement. NPS measurements were performed for three dose levels each between 71 µGy and 550 µGy air kerma in the image plane. MTF was determined only at the respective central dose levels, i.e. 141 µGy to 278 µGy. Anti-scatter grid and compression paddle were retracted or removed during all measurements.

The second investigated system was a Sectra Microdose Mammography (MDM) unit in clinical use in the Klinikum Starnberg in Germany. One specialty of this system is its scanning geometry. X-rays from its W/Al source are collimated to slits. After compression, the collimator is moved close to the compression paddle. For an examination, collimator and detector are scanned synchronously parallel to the breast wall across the imaging area, thereby effectively minimizing the effect of scattered radiation on the imaging process. The MDM's detector is an assembly of silicium strip detectors pointing in beam direction, mounted in a line perpendicular to the scan direction. It is operated in pulse counting mode with a threshold to suppress electronic noise. The two directions are referred to as scan direction and (detector) array direction below. The pixel size of 50 µm x 50 µm is defined by the strip geometry in array direction, and the combination of scan speed and integration time in scan direction. The MDM software normalizes each image, thereby preventing a direct measurement of the characteristic curve, yet its DICOM image headers include the respective individual normalization. With the characteristic curve type set to linear, it is possible to reconstruct image-specific curves.

The MDM geometry does not allow the upper mounting frame of the measurement setup to be placed between source and detector, since the collimator is moved to approximately 11 cm above the detector cover, regardless of compressed breast thickness. All necessary filters were therefore mounted directly on the collimator housing, while no machine-independent beam limitation could be mounted. The effect of lost beam limitation was investigated by using an additional lead shield as described below. The compression paddle was removed during measurements. The curved detector of the MDM prevented us placing the edge phantom as close to the detector as on typical flat detector systems. The phantom frame was mounted centrally in scan direction and parallel to its axis in array direction, resulting in a distance of up to 27 mm between detector cover and edge.

Voltage settings permitted by the Sectra standard software did not include 28 kV as recommend in IEC 62220-1-2, thus all measurements were performed at 29 kV. The investigated dose range covered the whole range available on the MDM, i.e. 6.5 – 25.8 mAs amounting to 97.2 – 378 µGy air kerma in the image plane. Dose variation was achieved by different scan times with a constant anode current setting of 180 mA according to the DICOM header information. Two sets of images were obtained; one by irradiating the full detector area, and a second one with a 2 mm lead shield placed on the MTF phantom frame approximately 6 cm above the detector cover in the central part of the detector, which limited the irradiated area to a field of 10 cm x 10 cm. The same regions of interest were used in both sets of images.

4.2 MTF, NPS and DQE of Sectra MDM

Figure 3 summarizes the MTF measurement results of the Sectra MDM. Beam limitation by the lead shield as compared to irradiation of the full detector area causes no significant difference in MTF over the whole frequency range up to the Nyquist frequency of 10 mm^{-1}. Scan and array direction results are clearly different. The MTF in array direction is slightly higher than that presented by Monnin et al.[1] and Honey et al.[2], which might be caused by slightly different placement of the MTF edge phantom. A comparison of measurements with identical edge position, but with the steel plate near to and far from the breast wall side, showed a relative deviation of 5 - 10 % over a large frequency range both with and without lead shield. The curve in figure 3 is the average of both curves as recommended by IEC 62220-1-2. In scan direction, the MTF is similar to Honey et al., but lower on average than both MTF curves measured by Monnin et al. The latter were obtained for different heights of the MTF phantom above the detector (0 mm and 50 mm), encompassing our placement of 27 mm above the cover. For most spatial frequencies, this difference is not covered by the respective uncertainties, which are ≤ 0.01 both for the results of Monnin et al. and the current measurement.

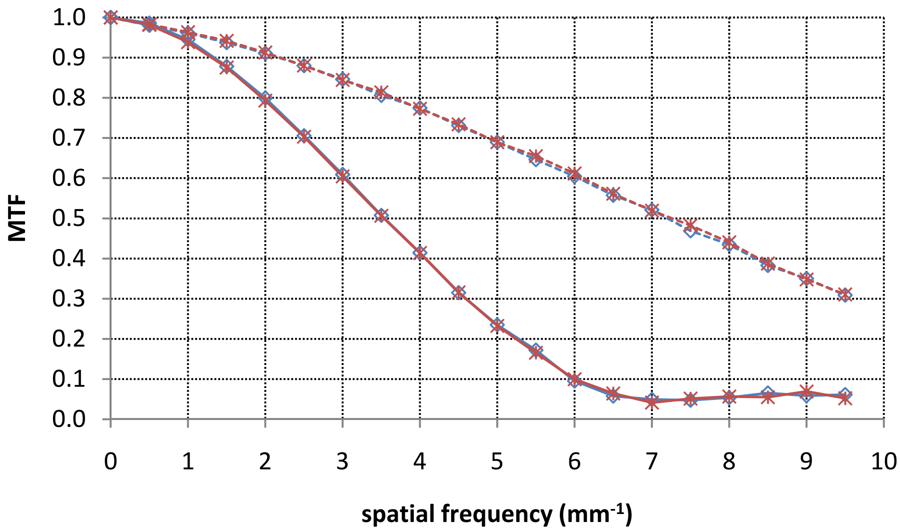

Figure 3: MTF results for Sectra MDM
Diamonds – full detector irradiated, stars – field limited by lead shield;
directions: scan – continuous line, array – dashed line; air kerma 191 μGy.

Figures 4 and 5 present the NPS results of the Sectra MDM. The NPS is relatively flat for both directions, which is in agreement with the NNPS presented by Monnin et al. and Honey et al., although the slope is slightly different in the array direction.

Beam shaping by the lead shield causes little overall difference, but results in a peak in scan direction, clearly observable at 378 μGy at 8.5 mm^{-1}, and also perceptible at 191 μGy and 4.5 mm^{-1}. A similar peak was also noted by Honey et al. at 5 mm^{-1}. A closer look at the NPS results exactly in scan direction also reveals a peak for the low dose level of 97.2 μGy in an image obtained with the lead shield. This is only discernible in high-resolution NPS data exactly on the frequency axis in scan direction, which is not included in the recommended IEC binning process. Figure 6 shows this data, normalized to the median NPS for each dose level, and with the spatial frequency axis scaled to the individual scan time. It also includes the similarly treated NPS derived from fully-irradiated parts of images used for MTF measurement without lead shield. In all four NPS curves, the highest value lies near a normalized spatial frequency of 0.55 $mm^{-1}\cdot s^{-1}$.

As stated above, dose variation in the Sectra MDM was achieved solely by changes in scan speed. The moving parts in the system are likely to excite vibrations. If vibrations at a specific frequency are intense enough to cause a feedback on the relative movement of detector and collimator, an interference pattern will occur in the recorded image, since the detector readout is also a periodic process. As the effect is only present with the MTF phantom placed on the detector, and more pronounced when the weight of the lead shield is added, we suppose that the supporting pins of the phantom frame define the dominant vibration frequency, similar to pitch variation on a string instrument. If this is true, the measurement setup has a noticeable effect on the measurement results, just by changes in the weight of the phantom support. IEC regulations are not clear enough to prevent this, since they do not specify how elements of the measurement setup should, or should not, be mounted on the systems under investigation. We consider such detailed regulations exaggerated, and would rather emphasize that our observation demonstrates how much caution must be used in measurement. Simply relying on a standard to produce repeatable and comparable results is obviously not justified.

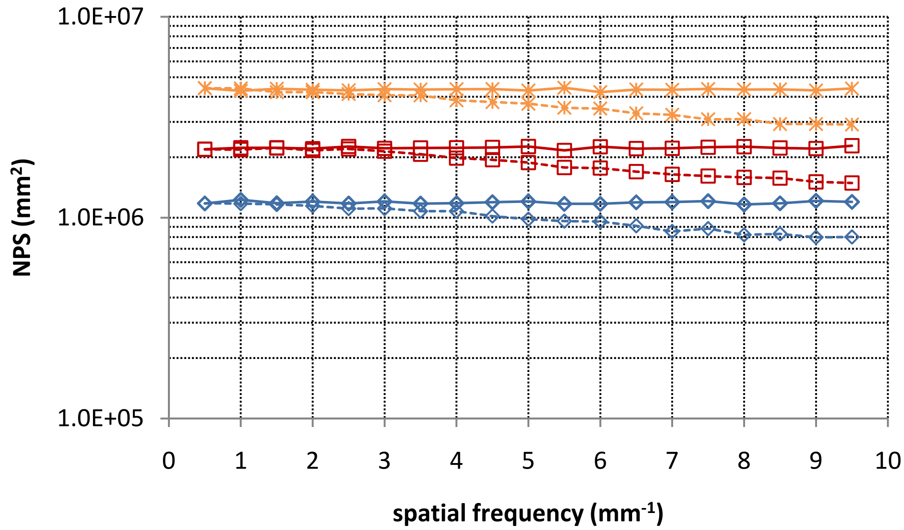

Figure 4: NPS results for Sectra MDM, full field irradiated
Diamonds 97.2 μGy, squares 191 μGy, stars 378 μGy; directions: scan – continuous line, array – dashed line

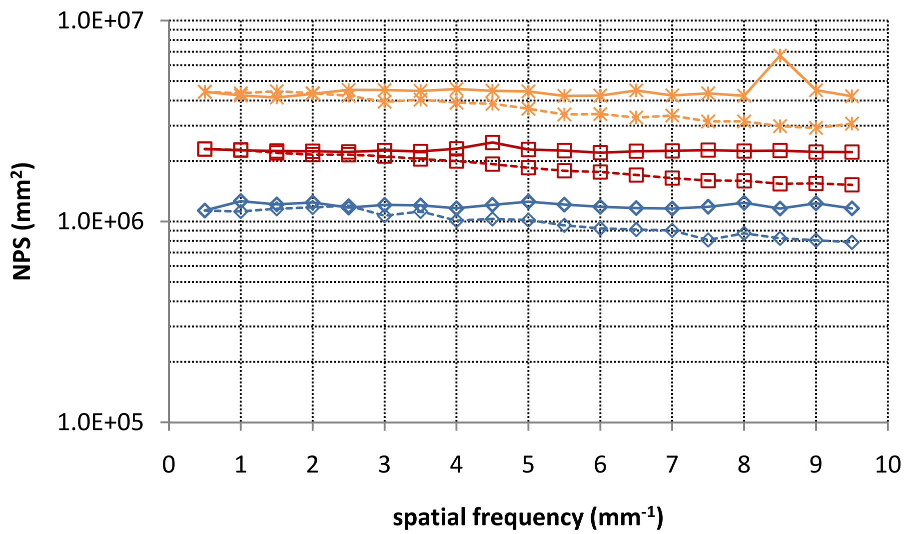

Figure 5: NPS results for Sectra MDM, x-ray field limited by lead shield
Diamonds 97.2 μGy, squares 191 μGy, stars 378 μGy; directions: scan – continuous line, array – dashed line

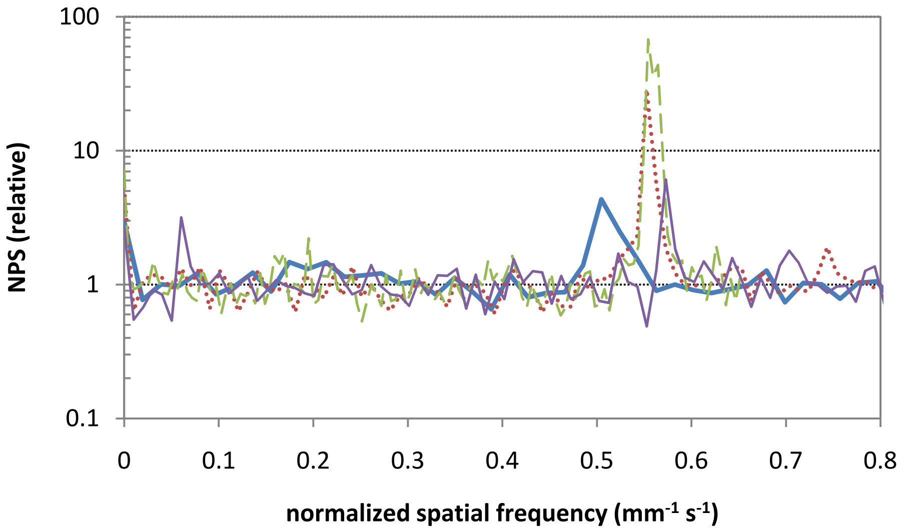

Figure 6: NPS peak in scan direction
See text for explanation; bold line – scan time 4.024 s, short dash – 7.774 s, long dash – 15.223 s,
all with lead shield on MTF phantom; thin line – scan time 7.774 s with MTF phantom but without lead shield

DQE results for the Sectra MDM are summarized in figures 7 and 8. Beam shaping by the lead shield causes a slight increase of the DQE in both directions at low spatial frequency. The DQE is slightly lower for 97.2 µGy than for both 191 µGy and 378 µGy. Peak DQE is similar to the results of Monnin et al. and Honey et al.

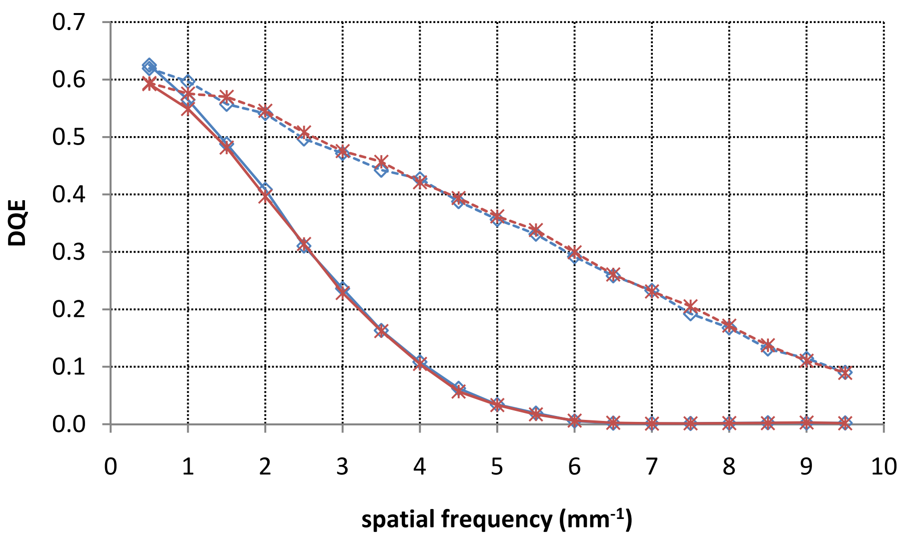

Figure 7: Effect of beam shaping on DQE
Diamonds – full detector irradiated, stars – field limited by lead shield;
directions: scan – continuous line, array – dashed line; air kerma 191 µGy.

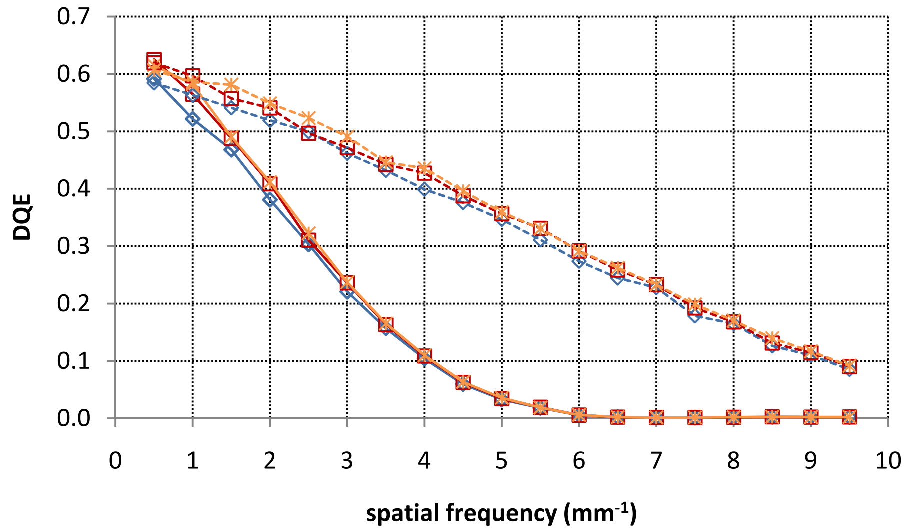

Figure 8: Dose dependence of Sectra MDM DQE
Diamonds 97.2 µGy, squares 191 µGy, stars 378 µGy; directions: scan – continuous line, array – dashed line

4.3 Uncertainties

Dosimetric corrections as defined in section 3 and their uncertainties vary little between the different measurements, since the geometric relations were similar. A list of these quantities is compiled in table 1.

With the exception of the Mo/Mo radiation quality at the Fujifilm Amulet, the half-value layer of all radiation qualities was thicker than the respective value listed in IEC 62220-1-2. Therefore, SNR_{in}^2 had to be modeled in most cases. Variation of inherent filtering thickness of Be, Al or Rh within plausible tolerances was not sufficient to attain the measured half-value layer. Good agreement between measured and modeled half-value layer thickness was accomplished by introducing a thin tungsten layer (3.8 – 6.4 µm W), representing anode roughening.

MTF and NPS uncertainties were calculated for each binned data point as described in section 3. Typically, MTF absolute uncertainties were approximately constant over the whole frequency range for the Fuijifilm Amulet, while in case of the Sectra MDM they increased slightly with higher spatial frequency. In both cases, the relative uncertainty increased with decreasing MTF from an average value of 0.3 % at 0 mm^{-1} to 3 % just below the Nyquist frequency. MTF absolute uncertainties were below 0.008, while the relative uncertainties reached values as large as 11 % if the MTF dropped below 0.1.

NPS relative uncertainties were independent of spatial frequency and dose on both systems as long as the linear approximation approach was valid, and ranged from 0.4 % to 3.3 %. In case of peaks or a nonlinear increase towards low spatial frequencies, relative uncertainties of up to 42 % were obtained, indicating a failure of the approximation approach, but also that the respective mean NPS values were invalid in the sense of IEC 62220-1-2.

Absolute DQE uncertainties with coverage factor 2 were always lower than the IEC-required value of 0.06, except when nonlinearities in the NPS occurred at low spatial frequency. However, especially in case of low DQE values at high spatial frequencies, some data points exceeded the relative uncertainty limit of 10 %.

Figure 9 shows the relative contribution of all components in equation (1) to the overall DQE variance. The curves are averaged from all measured data points, except those where the linear approximation approach for the NPS clearly failed due to nonlinear behavior. As long as SNR_{in}^2 values are directly adopted from IEC 62220-1-2 or at least normalized to those in the standard, their uncertainty is almost negligible, regardless of spatial frequency. NPS and air kerma uncertainties have an equal impact on the DQE variance (and thus, uncertainty) over the whole spatial frequency range, as long as the NPS features little curvature, and dominate DQE variance at low spatial frequency. With growing spatial frequency, MTF uncertainty grows in importance, amounting to up to 80 % of the total DQE variance close to the Nyquist frequency.

Table 1: Quantities relevant for dosimetry

	Range	Relative uncertainty (coverage factor 1)	Type (cf. GUM)
Electrometer reading: integrated charge - repeatability of exposure - additional uncertainty for low charge	 - -	 0.24 - 0.84 % 0.5 - 1 %	 A B
Calibration factor $N_k \cdot k_Q$	84.20 - 84.21 μGy·pC^{-1}	0.6 %	A
k_ρ	1.0116 - 1.1114	0.04 - 0.1 %	B
k_{Pos}	0.8108 - 0.8626	0.46 - 1 %	B
k_{Abs}	0.9943 - 0.9977	0.1 %	B
k_S	0.9885 - 0.9926	0.13 - 1 %	B
Air kerma	71.0 - 550 μGy	0.85 - 1.85 %	

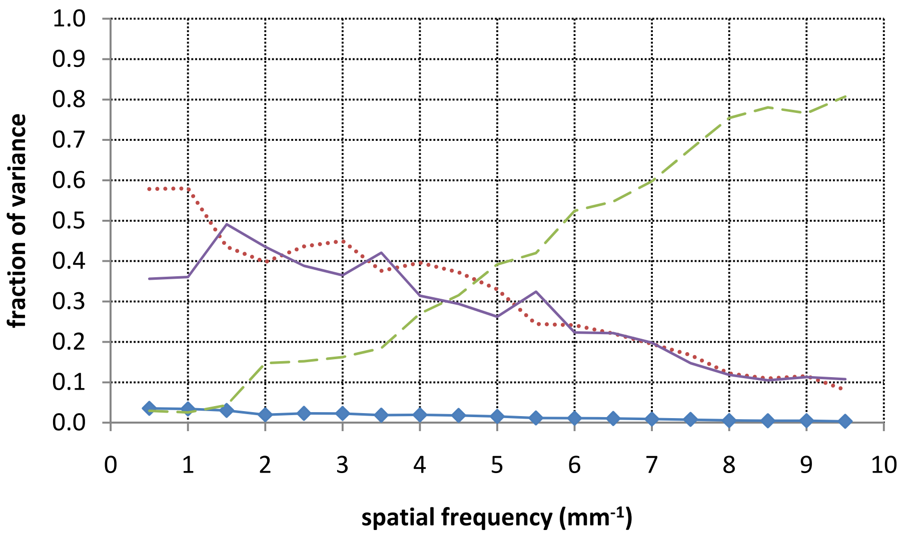

Figure 9: Relative composition of DQE variance
Line with diamonds - SNR_{in}^2, dotted line – air kerma, dashed line – MTF, continuous line - NPS

5. CONCLUSION

We presented a measurement setup for determination of the DQE of digital mammographic x-ray systems in accordance with the international standard IEC 62220-1-2. The measurement uncertainties obtainable with this setup and an adequate evaluation software suite fulfill the requirements of this standard.

MTF, NPS and DQE measurement results for a Sectra Microdose Mammography system in clinical use were comparable to, albeit slightly different from results previously published by other groups. By the example of a peak in the NPS in scan direction, it could be shown that closely following IEC 62220-1-2, variations in results may occur due to permitted variations in the measurement setup.

ACKNOWLEDGEMENTS

This work was primarily funded by the German Bundesministerium für Umwelt, Naturschutz und Reaktorsicherheit (BMU) through the Bundesamt für Strahlenschutz, Salzgitter, Germany, within its project StSch 4489 / 3608S04489. We are very grateful for the efforts of our center's workshop in construction of the measurement setup, and especially indebted to M. Scherer, who invested a lot of time, patience and good ideas. The authors would like to thank J. Spielmann and J. Müller at Fujifilm, as well as E. Mangel and I. Rieker in Starnberg for the access to the FFDM systems.

REFERENCES

1. Monnin, P., Gutierrez, D., Bulling, S. *et al.*, "A comparison of the performance of digital mammography systems," Medical Physics, 34(3), 906-914 (2007).
2. Honey, I., Lawinski, C., Blake, P. *et al.*, [Full Field Digital Mammography Systems. Sectra MicroDose. A technical report] NHS Purchasing and Supply Agency, Centre for Evidence-Based Purchasing (CEP), (2006).
3. IEC, [Medical electrical equipment - Characteristics of digital X-ray imaging devices - Part 1-2: Determination of the detective quantum efficiency - Detectors used in mammography], Geneva(2007).
4. ISO, BIPM, IEC *et al.*, [Guide to the expression of uncertainty in measurement (GUM)] International Organization for Standardization, Geneva(1995).
5. Hubbell, J. H., and Seltzer, S. M., [Tables of X-Ray Mass Attenuation Coefficients and Mass Energy-Absorption Coefficients (version 1.4)] National Institute of Standards and Technology, Gaithersburg, MD, (2004).
6. Cranley, K., Gilmore, B. J., Fogarty, G. W. A. *et al.*, [Catalogue of diagnostic X-Ray spectra and other data] Institute of Physics and Engineering in Medicine, York(1997).
7. Reilly, A. J., and Sutton, D., [Report 78 Spectrum Processor] Institute of Physics and Engineering in Medicine, York(1997).
8. Meyer, P., Buffard, E., Mertz, L. *et al.*, "Evaluation of the use of six diagnostic X-ray spectra computer codes," Br J Radiol, 77(915), 224-230 (2004).
9. Irisawa, K., Yamane, K., Imai, S. *et al.*, "Direct-conversion 50 μm pixel-pitch detector for digital mammography using amorphous Selenium as a Photoconductive Switching layer for signal charge readout." Proc. SPIE 7258(2009).